Evaluating Schmid criterion for predicting preferential locations of persistent slip markings obtained after very high cycle fatigue for polycrystalline pure copper

N.L. Phung, V. Favier *, N. Ranc

Arts et Métiers ParisTech, PIMM UMR CNRS 8006, 151 Bd de l'Hôpital, 75013 Paris, France

Available online 19 Marc 2015

Keywords:
Persistent slip bands
Grain boundaries
Finite element simulations
Elastic anisotropy
Crossslip

A B S T R A C T

Very high cycle fatigue carried out on pure copper polycrystals promotes early slip markings, labelled as slip markings of types II and III, localized close to grain or twin boundaries. In this work, we focus on whether Schmid criterion can predict the preferential sites of slip markings of types II and III and identify the active slip systems. Combining observations of slip markings and polycrystalline modeling, it is shown that considering pure cubic elastic behavior, maximum resolved shear stress as a criterion for type II slip markings preferential sites is 70% reliable criterion. Concerning slip markings of type III, the reliability falls to 30%. The role of cross slip is highlighted and a scenario rationalizing the stress amplitude conditions and sites to observe early slip markings of type II or III for copper polycrystals is proposed.

1. Introduction

There is currently a growing demand to investigate the Very High Cycle Fatigue (VHCF) regime (higher than 10^7 cycles) to improve the reliability of design calculations and to extend the service life. In this regime, the life span is mainly controlled by the crack initiation span. Using infrared thermography, Ranc et al. [1] showed that the crack propagation stage constitutes only 0.1% of the specimen life in VHCF in the case of high strength steel. The crack leading to failure initiates at a subsurface inclusion as commonly observed for multiphase alloys labelled as type II materials [2]. For ductile single phase materials, labelled as type I materials [2], Mughrabi's model suggests that cracks initiate at the surface owing to the accumulation of very small but irreversible (non recoverable) plastic deformation over very large number of cycles [3]. In the case of polycrystalline pure copper, Stanzl-Tschegg et al. [4,5] showed that the number of cycles needed to form the early persistent slip markings increases with decreasing stress amplitudes. Here, "persistent slip markings" means that when the surface was electropolished after fatigue, the slip markings reappeared at the same sites on the specimen surface when cyclic loading was resumed. Recently, some of the authors [6] investigated polycrystalline pure copper the fatigue strength of which was about 90 MPa at 5×10^9 cycles. They observed three types of early persistent slip markings in terms of their morphology, their spatial distribution in the polycrystalline material and the stress amplitude ranges at which they predominantly appear. For stress amplitudes higher than 65 MPa, straight and long early persistent slip markings crossing the grains are mainly generated. They were called slip markings of type I and are considered as the persistent slip bands (PSBs) commonly formed in the low and high cycle fatigue regimes. For stress amplitudes ranging from 30 MPa to 65 MPa, persistent slip markings, labelled as slip markings of types II and III, were observed.

In low and high cycle fatigue, PSBs appear in grains well-oriented for plastic slip and are along one dominant direction. An analysis based on the maximum Schmid factor (and so which considers isotropic elasticity) predicts well the grains which have PSBs and the active primary slip system [7,8]. The PSB direction is the trace of the primary slip plane emerging on the specimen surface (Fig. 1). Considering that slip markings are associated with the primary active slip system [8], we are focussing here on whether Schmid criterion can predict the preferential sites of slip markings of types II and III and identify the active slip systems.

Concerning the slip markings of type II, a previous paper [9] briefly exhibited that an analysis based on the maximum resolved shear stress is relevant as soon as the stress heterogeneities due to elastic anisotropy are considered. Using the finite element method,

* Corresponding author. Tel.: +33 1 44 24 64 07.
E-mail addresses: ngoclam250@yahoo.com (N.L. Phung), veronique.favier@ensam.eu (V. Favier), nicolas.ranc@ensam.eu (N. Ranc).

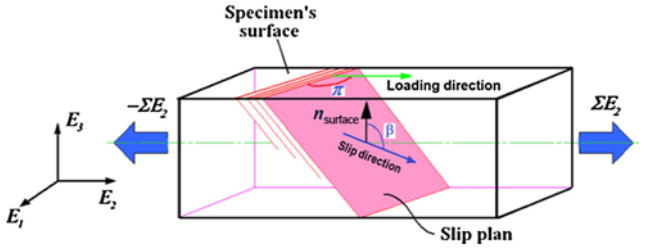

Fig. 1. A schematic isolated grain located at the specimen surface. The polycrystal which embeds the grain is subjected to uniaxial loading in the direction E_2. The angle π is the angle between the surface slip marking (trace of the primary slip plane which emerges on the surface) and the loading axis. The angle β is the angle between the slip direction of the slip system and the normal to the free surface.

the stress field was computed on a free surface where 2D grain shape and lattice orientation, coming from real microstructures, were explicitly represented. The plastic behavior was neglected. In this paper, results concerning slip markings of type II are explained in detail and the same method as in [9] is applied to evaluate Schmid criterion for predicting preferential sites of slip markings of type III. In addition, the reasons why twin boundaries promote slip markings are investigated. Section 2 recalls the main experimental results concerning the location and morphology of early slip markings of types II and III observed on pure copper specimen surface subjected to 20 kHz tension–compression fatigue tests [6]. While the Ref. [6] focused on local studies, a statistical approach is presented here to establish slip markings appearance criteria. Section 3 presents the based Schmid criteria and finite elements polycrystalline model. Only the cubic elastic behavior for the grains was considered. Section 4 gives the results obtained on copper bicrystals to investigate the role of the grain and twin boundaries on the stress heterogeneities and slip activity. Subsequently, the stress fields within real polycrystalline copper microstructure displaying slip markings of types II and III are computed. In Section 5, the validity of based Schmid criteria for predicted preferential sites of slip markings and the role of twin boundary are discussed. Finally, scenario and conditions for forming slip markings of types I, II and III are suggested.

2. Location and morphology of slip markings of types I, II and III

In a previous work [6], tension–compression fatigue tests in the VHCF regime were carried out on hour-glass shaped specimens made of oxygen-free high-conductivity commercially pure (99.95%) polycrystalline copper. All specimens were mechanically and subsequently electrolytically polished to remove residual stresses. To perform experiments up to a very high number of cycles in a reasonable time, ultrasonic equipment at a testing frequency of 20 kHz was used. The fatigue strength was found about 90 MPa at 5×10^9 cycles. Besides, fatigue loadings were interrupted repeatedly in order to perform surface studies by optical microscopy, scanning electron microscopy (SEM), electron back scattering diffraction (EBSD) technique and atomic force microscopy (AFM) after different numbers of cycles. The [30–65 MPa] stress amplitude range was chosen much smaller than for the stress–number curve to observe the early traces of plasticity on the surface specimen. EBSD analyses clarified the places of the plastic markings with regard to the polycrystalline microstructure. AFM was operating directly to the surface specimen to keep the details of the height of the slip markings. Fig. 2 exhibits the stress amplitude needed to form the early slip markings as a function of the number of cycles. Three types of early persistent slip markings in terms of their morphology, their spatial distribution in the polycrystalline material and the stress amplitude ranges at which they predominantly appear were distinguished. A scheme of their

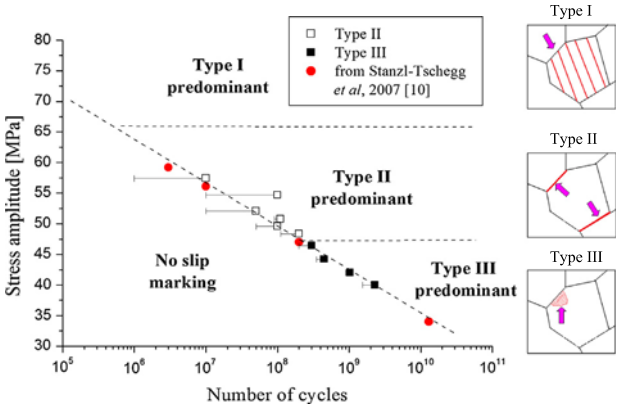

Fig. 2. Stress amplitude needed to form the early slip markings of types I, II and III and scheme of their location as a function of the number of cycles (from [6]).

location with regard to the polycrystalline microstructure is given in Fig. 2. For stress amplitudes higher than 65 MPa, straight and long early persistent slip markings crossing the grains are mainly generated. They were called slip markings of type I and are considered as the classical persistent slip bands (PSBs). For stress amplitudes ranging from 45 MPa to 65 MPa, most of early slip markings are straight and long but located near and along twin boundaries oriented at about 45° from the loading direction. They are called persistent slip markings of type II. For stress amplitudes below 45 MPa, clusters of fine and short early persistent slip markings of type III are mostly produced and located near grain boundaries and triple junctions. Their height is less than 50 nm while it is about 1 μm for the slip markings of types I and II. On the contrary to the slip markings of types I and II, two slip marking directions were usually observed. The first one is more marked and occupies most cluster surface. No slip markings were observed for stress amplitude lower than ~30 MPa up to 10^{10} cycles. Further details are given in [6]. While the Ref. [6] focused on local studies, a statistical approach is presented here to establish slip markings appearance criteria. Four 170 μm × 170 μm zones of interest containing 192 grains and 11 slip markings of type II in all and three 80 μm × 80 μm zones of interest containing 204 grains and 11 slip markings of type III in all were investigated using SEM and EBSD techniques to analyze the location and orientation of the 22 slip markings with regard to the polycrystalline microstructure. Results are presented in Section 4.2.

3. Method: presentation of the criteria for slip markings and numerical polycrystalline model

3.1. Based Schmid criteria

Pure copper has a face-centered cubic (FCC) crystalline structure. Table 1 recalls the 12 $\{111\}\langle 110\rangle$ slip systems using Schmid and Boas notations [10].

An isolated grain located at the specimen surface as schematically presented in Fig. 1. The polycrystal which embeds the grain is subjected to uniaxial loading in the direction E_2. When considering crystalline cubic elastic behavior, the components σ_{ij} of the local stress tensor within a grain varies from one point to another and the local resolved shear stress τ^s of the slip system S is calculated by the Eq. (1):

$$\tau^s = R^s_{ij}\sigma_{ij} \tag{1}$$

where R^s_{ij} are the components of the Schmid tensor of the slip system S. When considering isotropic elastic behavior, all grains have the same elastic response despite of their different orientation.

Table 1
Notations of Schmid and Boas in FCC material [10].

Slip plan	Slip direction						Possible slip systems		
A: $(\bar{1}11)$							A2	A3	A6
B: (111)	1	2	3	4	5	6	B2	B4	B5
C: $(\bar{1}\bar{1}1)$	$[011]$	$[0\bar{1}1]$	$[101]$	$[\bar{1}01]$	$[\bar{1}10]$	$[110]$	C1	C3	C5
D: $(1\bar{1}1)$							D1	D4	D6

The local stress tensor components are equal to the applied stress tensor components Σ_{ij}. The only component not zero is $\Sigma_{22} = P$. The local resolved shear stress τ^s of the system S at any point of grain is equal to (2):

$$\tau^s = R^s_{22} P \tag{2}$$

where R^s_{22} is the Schmid factor of the slip system S corresponding to the uniaxial loading in the direction E_2.

To correlate slip markings and slip systems, the resolved shear stress τ^s was calculated according to both Eqs. (1) considering cubic elasticity or (2) considering isotropic elasticity. Real polycrystalline microstructures were geometrically represented and discretized to compute the stress field using finite element method. For each grain, the maximum resolved shear stress was identified and location at which it was found was noted. In some cases, two very close values were found. To determine the active slip system, the angle π between the trace of slip marking on surface and the loading axis (Fig. 1) was measured. This measured angle π was compared with the calculated π of the $\{111\}\langle 110\rangle$ slip systems. The slip system having the highest resolved shear stress and similar angle π to the experimental one was considered to be the active slip system according to the Schmid criterion.

3.2. Numerical polycrystalline model

Quasi 3D finite element simulations were carried out using the ABAQUS software and considering the orientation, the shape and the cubic elastic behavior of each grain. Quasi 3D simulations are in the sense that the third geometrical direction was extruded from one specimen surface. The plastic behavior is neglected since we are just interested in the early slip markings appearance for which the material is mainly elastic. The elastic constants in each grain are determined by the crystal orientation and the standard elastic constants of copper single crystal, C_{11} = 168.4 GPa, C_{12} = 121.4 GPa and C_{44} = 75.4 GPa [11]. Perfect bonding condition is imposed to the interface between grains.

3.2.1. Model for copper bicrystals

Bicrystals are studied to simplify the problem and investigate the effect of misorientation and grain boundary orientation with regard to the loading direction on the stress field. Three bicrystals, here after named G1–G2, G3–G2 and G4–G2, were considered. The grain called G2 was combined with the grains G1, G3 and G4, respectively. Real twin-matrix bicrystal was also studied. The geometry, boundary conditions and mesh for the bicrystals G1–G2, G3–G2 and G4–G2 are given in Fig. 3. The width a and the thickness b were both 10 μm. Their length L was 30 μm. E_2 is the tensile and specimen axes. The grain boundary crossed the bicrystals along the direction E_3. It was inclined α degrees from the tensile axis in the front and opposite faces normal to E_3. G1 is oriented as a twin with regard to G2. The misorientation calculated according to [12] is 60° and both G1 and G2 contain a common slip plane (the slip plane B for the grain G1 and the slip plane C for the grain G2) which have the same angle $\pi = 135°$. In a real twin-matrix case, this shared slip plane is also the twin boundary plane. Here, as the twin boundary plane crossed the bicrystal along the direction E_3, G1–G2 represents the twin-matrix case only from a 2D point of view but neglects the 3D aspect. This issue is discussed in Section 4.1.3. G3 is a common grain with regard to G2. The corresponding misorientation is 39°. At last, the misorientation between the two grains G2 and G4 is ~60° but they are not twin-matrix in the sense that they have not common slip plane with the same angle π.

A uniform tensile uniaxial stress P was applied on the two faces normal to E_2. The other surfaces were free. In 2D and 3D linear elasticity, the stress field tends to infinite when approaching an interface (such as the present grain boundary) intersecting a free surface [13]. The slip markings or cluster of slip markings of interest are 1–5 μm wide [6]. Consequently, averaged stress values over 1 μm × 1 μm are relevant to correlate stress heterogeneities and slip markings. The step size of the discretization grid was thus chosen close to 1 μm to sort out the elastic singularity issue and be consistent with the wanted microstructural information. For the bicrystals, the finite elements were linear quadrangle and their maximum size is 0.5 μm. The crystalline orientation of the grains, the angles π and Schmid factors R_{22} for the $\{111\}\langle 110\rangle$ slip systems are given in Table 2. The crystalline orientation is represented by the Euler angles φ_1, Φ, φ_2 defined by Bunge and Esling [14]. Three successive rotations φ_1, Φ, φ_2 transform the crystal axes in the crystal coordinate system so that they coincide with that of the sample coordinate system. As a result, the crystalline orientation of the grain is given by the rotation matrix M_D:

$$M_D = \begin{bmatrix} \cos\varphi_1\cos\varphi_2 - \sin\varphi_1\sin\varphi_2\cos\Phi & \sin\varphi_1\cos\varphi_2 + \cos\varphi_1\sin\varphi_2\cos\Phi & \sin\varphi_2\sin\Phi \\ -\cos\varphi_1\sin\varphi_2 - \sin\varphi_1\cos\varphi_2\cos\Phi & -\sin\varphi_1\sin\varphi_2 + \cos\varphi_1\cos\varphi_2\cos\Phi & \cos\varphi_2\sin\Phi \\ \sin\varphi_1\sin\Phi & -\cos\varphi_1\sin\Phi & \cos\Phi \end{bmatrix}$$

3.2.2. Model for copper polycrystals

Evaluating Schmid criteria for predicting preferential sites for the slip markings of types II and III requires to compute the stress field for real polycrystalline microstructure. The procedure used to carry out quasi 3D finite element simulations is illustrated in Fig. 4. Real copper polycrystalline microstructures were obtained from EBSD maps. Grain boundaries were identified as regions with >5° misorientation with neighboring points to get grain maps including about 50 grains each (Fig. 4c). The grain maps visualize the central part, where the stress amplitude is the highest in the flat specimen front face loaded in tension/compression in the VHCF

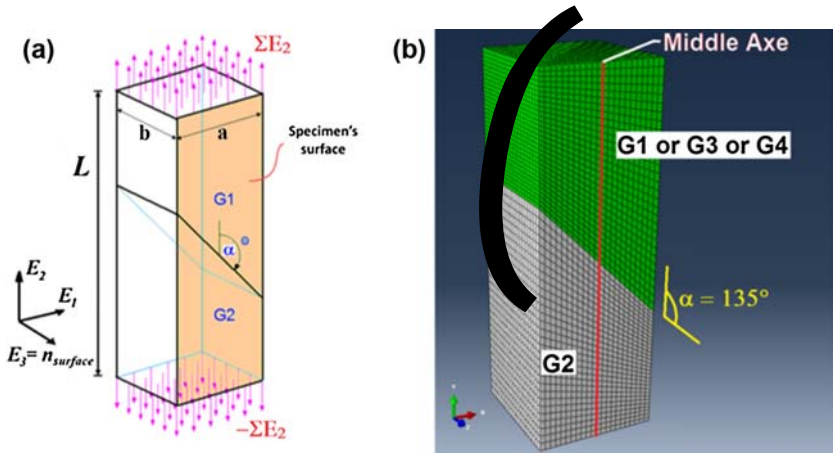

Fig. 3. (a) Geometry and boundary conditions of studied bicrystals; (b) associated mesh.

Table 2
Orientation, Schmid factors and angles π for the grains used in the bicrystal simulations and misorientation between G1–G2, G3–G2 and G4–G2. Misorientation was calculated according to [12]. The maximal Schmid factors are printed in bold.

G1 (misorientation with G2 = 60°, twin with G2 only from 2D point of view, common plan with G2: plan B)													
0:3078 −0:8158 −0:4896		B5	**B4**	B2	A6	A3	A2	D6	D4	D1	C5	C3	C1
@ −0:8526 −0:4649 0:2387 A	π	135°	135°	135°	24°	24°	24°	1°	1°	1°	94°	94°	94°
−0:4223 0:3439 −0:8387	R_{22}	0.13	**0.44**	0.31	0.36	0.13	0.23	0.0	0.0	0.0	0.23	0.31	0.08
G2 (twin with G1, common plan with G1: plan C)													
0:2224 0:9685 −0:1123		B5	B4	B2	A6	A3	A2	D6	**D4**	D1	C5	C3	C1
@ 0:9525 −0:1913 0:2368 A	π	156°	156°	156°	55°	55°	55°	62°	62°	62°	135°	135°	135°
0:2079 −0:1596 −0:965	R_{22}	0.29	0.28	0.00	0.42	0.44	0.02	0.31	**0.46**	0.14	0.44	0.31	0.13
G3 (misorientation with G2 = 39°)													
0:3816 0:7498 −0:5406		B5	B4	B2	**A6**	A3	A2	D6	D4	D1	C5	C3	C1
@ 0:3653 0:4149 0:8333 A	π	158°	158°	158°	46°	46°	46°	12°	12°	12°	86°	86°	86°
0:8491 −0:5154 −0:1155	R_{22}	0.09	0.34	0.25	**0.40**	0.08	0.32	0.09	0.09	0.01	0.23	0.16	0.07
G4 (misorientation with G2 = 60° but not twin-matrix)													
0:7805 0:2825 −0:5577		**B5**	B4	B2	A6	A3	A2	D6	D4	D1	C5	C3	C1
@ 0:5382 −0:7575 0:3695 A	π	47°	47°	47°	109°	109°	109°	80°	80°	80°	176°	176°	176°
−0:318 −0:5886 −0:7432	R_{22}	**0.45**	0.38	0.07	0.32	0.2	0.11	0.09	0.16	0.25	0.05	0.01	0.06

regime (Fig. 4a). They include slip markings (Fig. 4b). 2D meshes were constructed from the knowledge of the grain shape and crystal orientation at the specimen front surface (Fig. 4d and e). The 20 μm thickness of the grains was extruded from the surface. The finite elements are linear triangle and their edges were about 1 μm. A uniform tensile uniaxial stress was applied on the two faces normal to the loading direction (Fig. 4d). The four others surface were stress free.

3.2.2.1. Investigating slip markings of type II. Four 170 μm × 170 μm zones of interest (called A, B, C, D) were chosen because they contained slip markings of type II (Fig. 5 left). The latter are in black on grain maps due to unresolved crystal indexation in these strongly strained areas. The four zones were obtained from a polycrystalline copper specimen 20 kHz cyclically loaded at 56.4 MPa stress amplitude after 10^7 cycles. Considering the four zones, the total number of grains is 192. The total number of grains with slip markings of type II is 11.

3.2.2.2. Investigating slip markings of type III. Investigation of slip markings of type III was carried out on a polycrystalline copper specimen cyclically loaded at 49.6 MPa stress amplitude up to10^8 cycles. Three 80 μm × 80 μm zones of interest (called K, L, M) were chosen because they contained slip markings of type III (Fig. 6). They included 204 grains and 11 slip markings of type III.

4. Results

4.1. Copper bicrystals

4.1.1. Effect of misorientation on stress heterogeneities near grain boundary

The profiles of the component σ_{22} of the local stress tensor normalized by the applied stress Σ (σ_{22}/Σ) (Fig. 7a) and the maximum resolved shear stress normalized by Σ ($\tau_{max}=$) (Fig. 7b) were plotted along the length of the bicrystals. The values were taken along the middle axis of the front surface to avoid edge effects. Fig. 7c is a focus on Fig. 7b in the vicinity of the grain boundary and indicates the slip system associated with the maximum resolved shear stress. For these simulations, the angle α is 135°. σ_{22} is equal to Σ from the ends of the specimen up to about 10 μm of the grain boundary. When approaching to the grain boundary, σ_{22}/Σ steeply changes and is discontinuous at the oblique grain boundary. It was also observed that the local stress tensor is uniaxial far from grain boundaries and become triaxial close to grain boundary. The triaxiality values at grain boundaries were found equal to 0.14 and 0.36 for the grains G1 and G2, respectively. They were found equal to 0.29 and 0.38 for the grains G3 and G2 and 0.28 and 0.40 for the grains G4 and G2, respectively. Note that 0.33 is the triaxiality value for uniaxial stress state. The $\sigma_{22}/$ profile in G2 near the grain boundary was found to depend on the

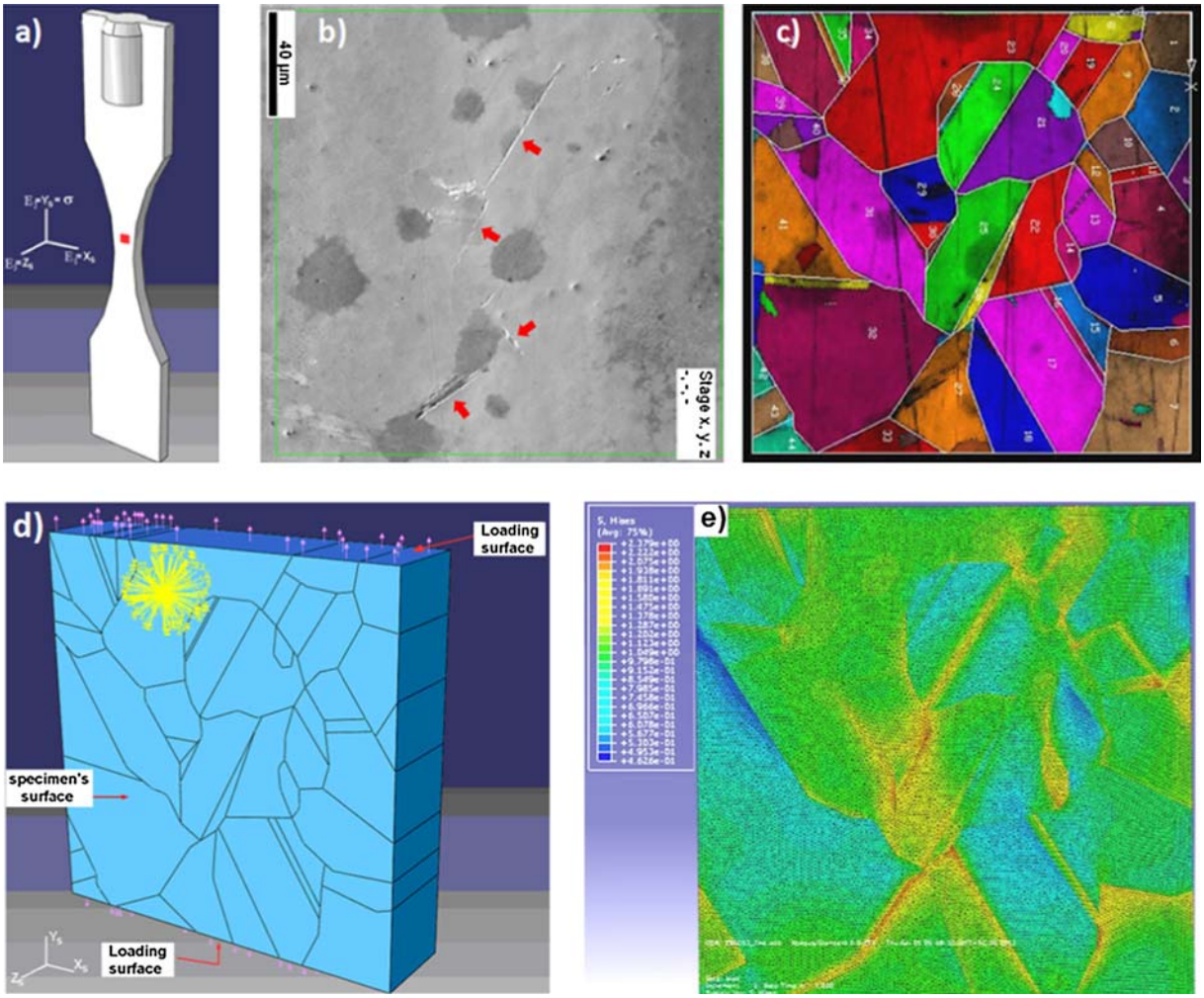

Fig. 4. Schematic illustration of the finite element simulation procedure: (a) specimen geometry used for VHCF tests and definition of the main axis – the small square drawn on the specimen surface indicates the location of the subsequent from (b) to (e); (b) scanning electron micrograph of a zone in the central part of the specimen front surface (the zone contains some slip markings of type II); (c) grain map from EBSD analysis of the same zone; (d) explicit representation of the polycrystalline microstructure of the same zone and boundary conditions used for finite element simulation; (e) mesh and von Mises stress field computed with finite element simulations.

orientation of the neighboring grain: σ_{22}/Σ steeply increases for the bicrystal G1–G2 while it does not change much for G3–G2 and G4–G2. The non-homogeneity of the stress field straightly impacts the maximum resolved shear stress and the active slip systems. Far from the grain boundary, the slip system having the highest resolved shear stress is the slip system having the highest Schmid factor as expected since σ_{22} is around Σ. This slip system is B4, D4, A6 and B5 for the grains G1, G2, G3 and G4, respectively (printed in bold in Table 2). When approaching the grain boundary, the active slip systems does not change for the grains G1, G3 and G4. However, it changes for the grain G2 from D4 to C5, A6 or A3 for the bicrystal G1–G2, G3–G2 and G4–G2 respectively. Concerning the bicrystal G1–G2, it is worth noticing that the angle π of the active slip systems at the grain boundary is 135° in both grains (B for the grain G1 and C for the grain G2). They correspond to the trace of the grain boundary in this simulation ($\alpha = 135°$). These results show that the stress field, the resolved shear stress and also, the active slip system in the grain G2 change in the vicinity of grain boundary depending on the neighboring grain orientation.

4.1.2. Effect of grain boundary angle on stress heterogeneities near grain boundary

Systematic calculations involving various α ranging from 40° to 140° were carried out for the three bicrystals to look for impact of α on the stress heterogeneities and active slip systems. Fig. 8 reports the maximum resolved shear stress $|\tau_{max}^{P}|$ and active slip system at the grain boundaries. The maximum resolved shear stress was found to depend on α. The active slip system B4 for the grain G1 does not change with α. However, the active slip system for the other grains changes with α: it is D4, A6, A3 or C5 for the grain G2, it is B4, A2 or A6 for the grain G3 and B5 or B4 for the grain G4.

4.1.3. Twin boundary case

Let us consider the real twin-matrix case called $G1_{twin}$–G2 bicrystal. Fig. 9a displays a similar configuration to the G1–G2 bicrystal but the twin boundary is inclined $\alpha = 135°$ from the tensile axis in the front face normal to E_3 and $\gamma = 40°$ from the tensile axis in the face normal to E_1. To keep a loaded upper surface into the grain $G1_{twin}$, the height of the bicrystal was increased from 30 µm to 40 µm (Fig. 9a). Fig. 9b compares the σ_{22}/Σ profiles for both bicrystals. At grain boundary, σ_{22}/Σ is slightly higher for $G1_{twin}$–G2 than G1–G2 (1.48 and 1.45) and is the highest among the four studied cases. Fig. 9c reports the corresponding resolved shear stress $|\tau_{max}^{P}|$ and active slip system near grain boundary. It shows that the active slip systems are not different for both cases. Far from grain boundary, it is B4 for G1 and D4 for G2. At the grain boundary, it is B4 for G1 and C5 for G2. The two latest are parallel to the twin boundary plane. Nevertheless, the resolved shear stresses $|\tau_{max}^{P}|$ (0.73 and 0.7 for the grains G1 and G2,

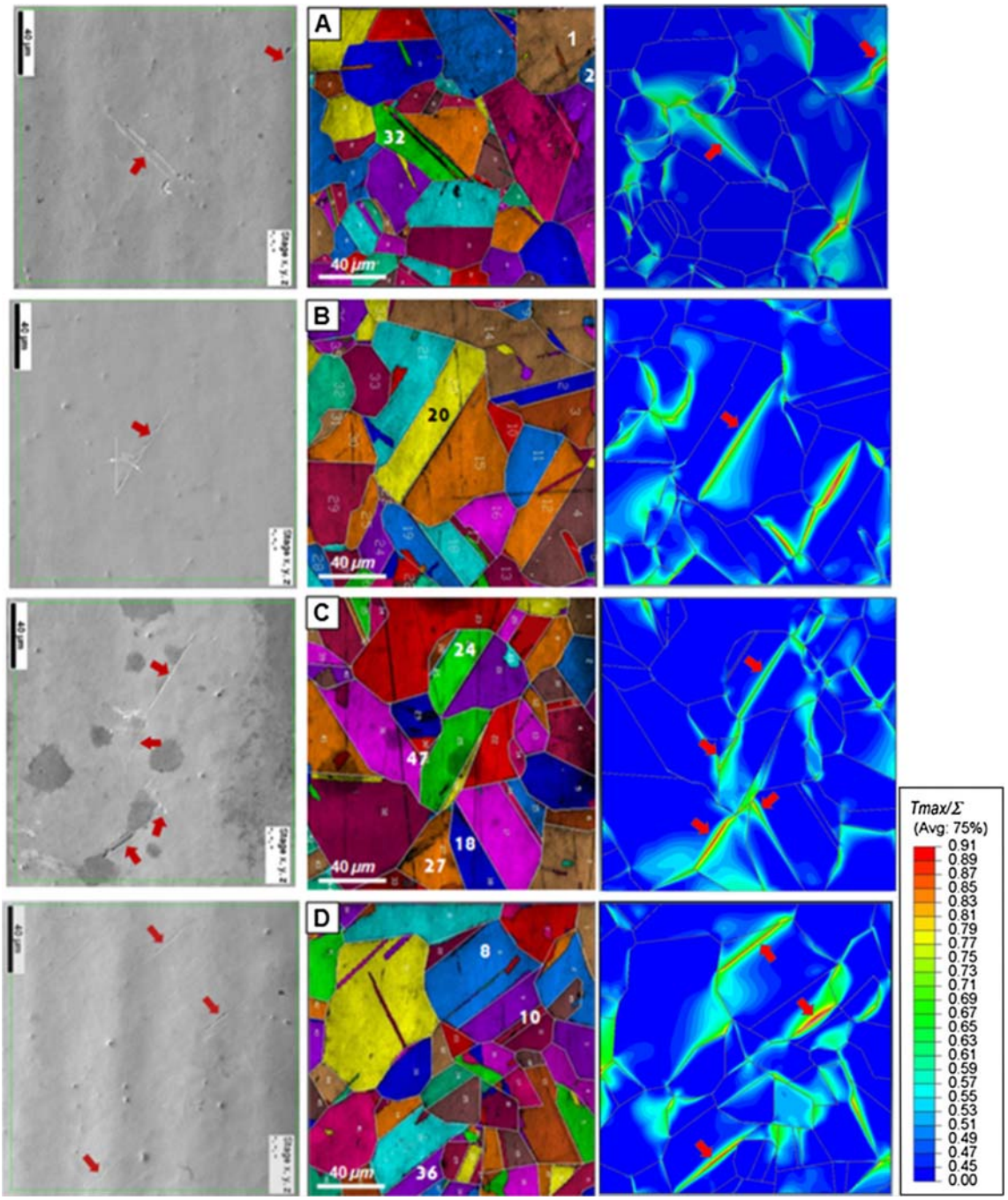

Fig. 5. SEM images (on the left) and grain maps (in the middle) of the four studied zones (A, B, C, D) obtained from a specimen loaded at 56.4 MPa stress amplitude up to 10^7 cycles using a 20 kHz – ultrasonic device. Maximum resolved shear stress normalized by the applied stress ($|\tau_{max}^{p}|$) maps (on the right) calculated by finite element simulations assuming crystalline cubic elastic behavior. The loading axis is vertical.

respectively) at the grain boundary for the $G1_{twin}$–G2 bicrystal are found much higher than for the G1–G2 bicrystal (0.55 and 0.6 for the grains G1 and G2, respectively).

4.2. Copper polycrystals – comparison with experiments

4.2.1. Slip markings of type II

The absolute values of the local maximum resolved shear stresses normalized by the applied stress $|\tau_{max}^{p}|$ were computed within the four zones A, B, C, D displaying slip markings of type II (Fig. 5). A very good match was found between places with the highest maximum resolved shear stress and slip marking sites. Note that the mechanically affected twin boundary area is found very small (~5 µm) as illustrated in the highest resolved shear stress map of zone B at the location indicated by the arrow (Fig. 5).

Fig. 10 displays the number of grains having $|\tau_{max}^{p}|$ equal to a given value ($|\tau_{max}^{p}|$ histogram over 192 grains). The range of $|\tau_{max}^{p}|$ was divided into intervals of 0.02 except for the first interval which includes values between 0 and 0.35. As mentioned above, 11 of 192 grains exhibited one slip marking. These grains are indicated by the following notation: G number of the grain/label of the zone (A, B, C or D). For example, G32/A means one slip marking in the grain numbered 32 belonging to the zone A. In addition, the maximum Schmid factor was calculated for each

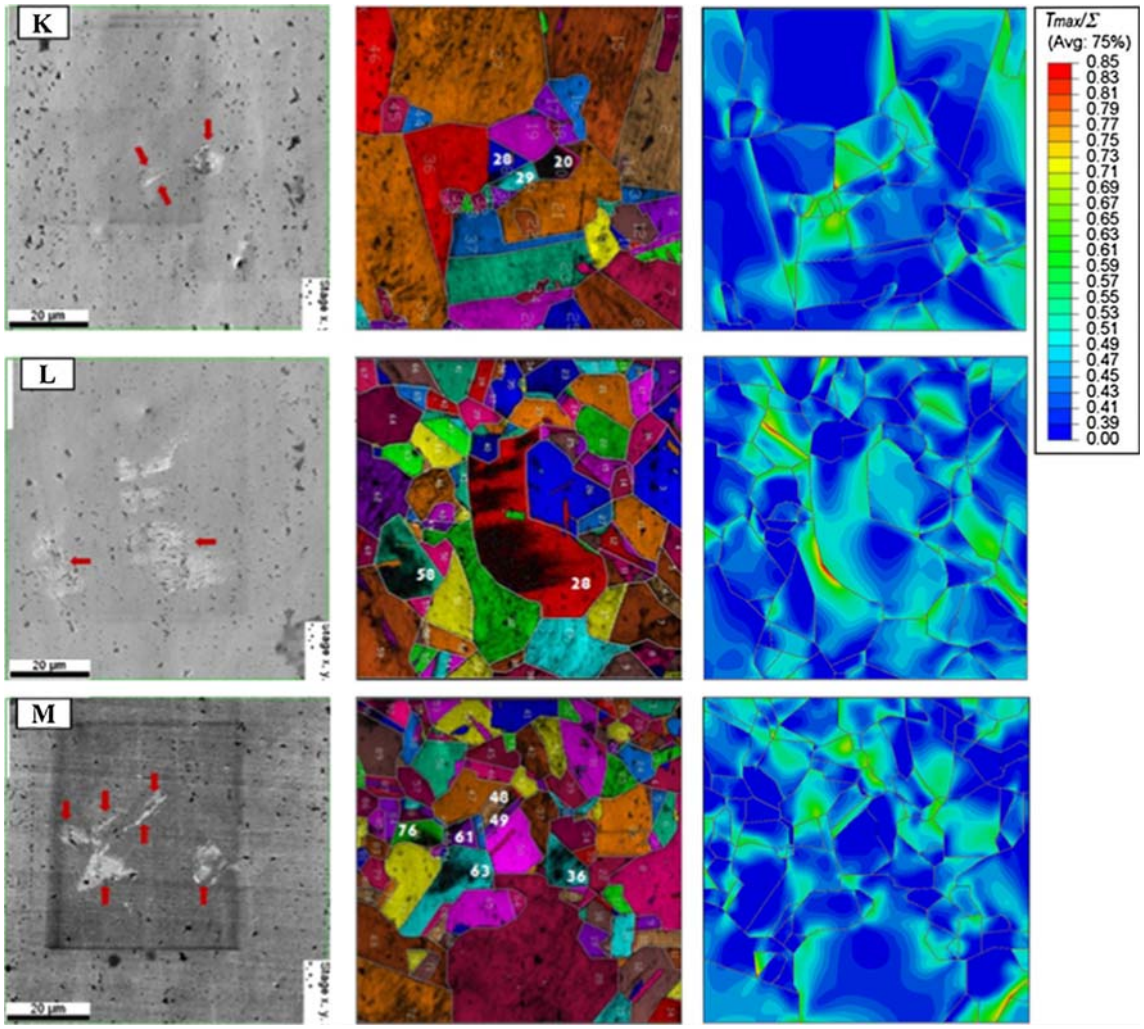

Fig. 6. SEM images (on the left) and grain maps (in the middle) of the three studied zones obtained from a specimen loaded at $\Delta\sigma/2$ = 49.6 MPa up to10^8 cycles using a 20 kHz – ultrasonic device. Maximum resolved shear stress normalized by the applied stress ($|\tau_{max}^{P}|$) map (on the right) calculated by finite element simulations and assuming crystalline cubic elastic behavior. The loading axis is vertical.

grain. Note that, while the Schmid factor is limited to values between 0 and 0.5, $|\tau_{max}^{P}|$ calculated assuming cubic elasticity reaches 0.9 because of the stress concentration or/and triaxiality.

The maximum Schmid factor for the grains having one slip marking was in the range of 0.44 and 0.5. However, in this range, many other grains (115 grains) do not have any slip marking. This result demonstrates that considering the maximum Schmid factor is not enough selective to predict the grains having one slip marking of type II. Besides, it was checked that the predicted primary active slip system is wrong for four cases (G32/A, G20/B, G24/C, G47/C) because slip activity changes near grain twin boundaries.

Considering cubic elasticity, $|\tau_{max}^{P}|$ for the grains having one slip marking was in the range of 0.78 and 0.9. In that case, only four other grains have $|\tau_{max}^{P}|$ in this range and do not have any slip band. This result shows that, considering cubic elasticity, maximum resolved shear stress as a criterion for type II slip markings preferential sites is 70% (11 of 15 grains) reliable criterion.

The previous analysis also revealed that the 11 slip markings of type II are located at or very close to a grain boundary whose misorientation is very high from 58.5° to 60°. Nine (9 of 11) of these markings appeared at or very near a twin boundary (G1/A, G2/A, G32/A, G20/B, G18/C, G24/C, G47/C, G36/D and G10/D). The corresponding slip plane is parallel to the twin boundary plane. For the last two slip markings (G27/C and G8/D), the grain boundary is not a twin boundary, although the misorientation is close to 60°. The involved twin boundaries were inclined from 24° up to 53° from the loading axis. Besides, the Schmid criterion accounting for crystalline cubic elasticity successfully predicts the primary active slip system.

4.2.2. Slip markings of type III

The absolute values of the local maximum resolved shear stresses normalized by the applied stress $|\tau_{max}^{P}|$ were computed within the three zones K, L, M displaying slip markings of type III (Fig. 6). The match between places with the highest maximum resolved shear stress and slip marking sites is not as good as for the slip markings of type II. For instance in the zone L, the presence of slip markings in the grain G28/L correlates well with the high value of $|\tau_{max}^{P}|$. On the opposite, there is no clear correlation between the presence of slip markings and $|\tau_{max}^{P}|$ in the grain G58/L. Combining slip markings observations and finite element study, it is concluded that the slip markings of type III were mainly observed near high-angle grain boundaries where resolved shear stresses were found the highest. As for slip markings of type III, the high-angle grain boundaries are twin boundaries for 7 of 11 cases: G20/K, G28/K, G29/K, G58/L, G48/M, G49/M and G63/M.

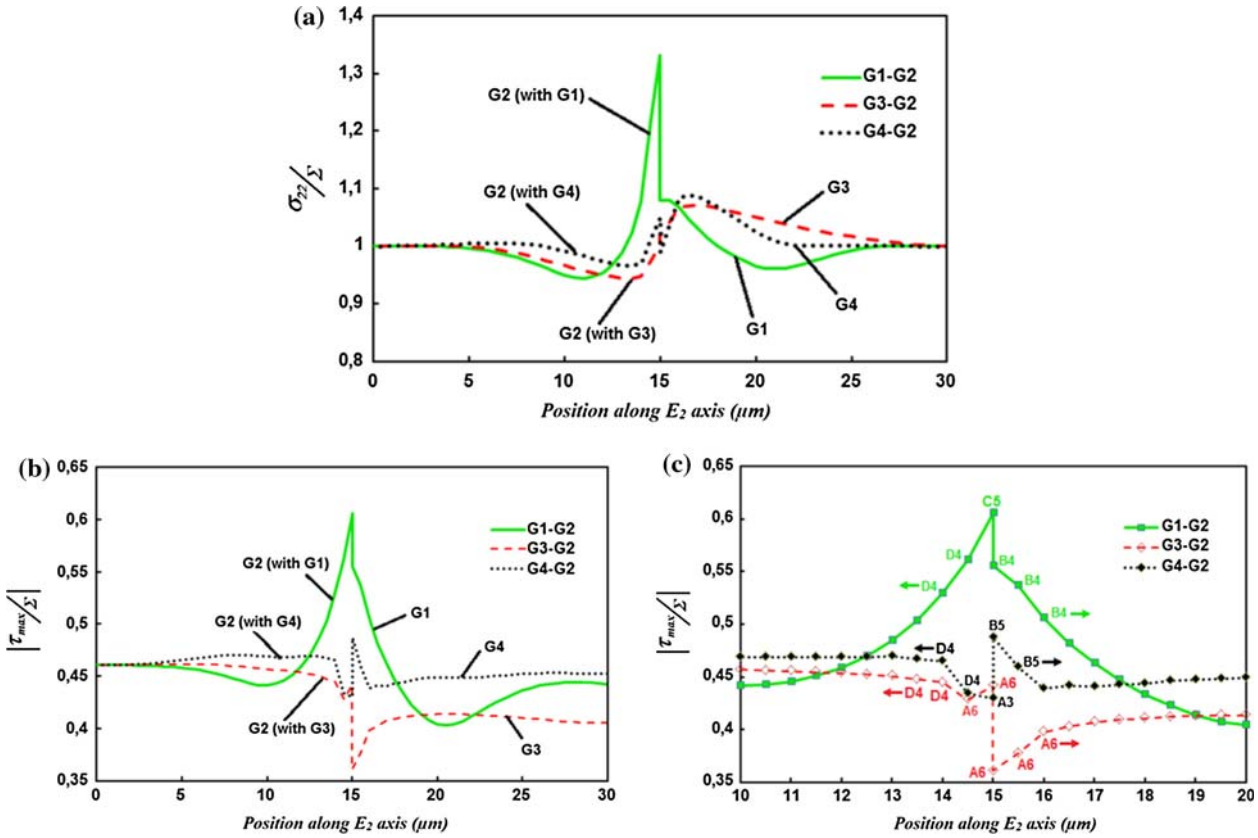

Fig. 7. Profiles of stress normalized by the applied stress Σ along the middle axis of the front surface for bicrystals G1–G2, G3–G2 and G4–G2 – (a) profile of σ_{22}/Σ – (b) profile of $|\tau_{max}^{p}|$ – (c) focus on (b) in the vicinity of the grain boundary position and slip systems the slip systems associated with the maximum resolved shear stress.

Grain boundary misorientation ranges between 45° and 53° for 4 other cases (G28/L, G36/M, G61/M, G76/M).

The $|\tau_{max}^{p}|$ histogram over 204 grains contained into the three zones (K, L, M) is plotted in Fig. 11. Considering isotropic elasticity, the Schmid factor for the grains exhibiting slip markings of type III was in the range of 0.37 and 0.5. However, 189 grains without any slip marking also display Schmid factor between 0.37 and 0.5. Now, considering cubic elasticity, $|\tau_{max}^{p}|$ for the grains having slip markings of type III are the highest and in the range of 0.59 and 0.82. However, 39 grains without any slip marking still display $|\tau_{max}^{p}|$ in this range. Considering cubic elasticity, maximum resolved shear stress as a criterion for type III slip markings preferential sites is thus satisfied for 11 of 39 grains, namely for 30% grains.

Two slip marking directions were usually observed [6]. Fig. 12 exhibits slip markings belonging to the grain G20/K shown in Fig. 6. The slip markings corresponding to the first direction are more marked and occupy most cluster surface. They are very likely associated with the primary slip system. The second slip markings are less marked and are called secondary slip markings. The primary slip markings are inclined 28° while the secondary slip markings are inclined 156° from the loading axis (angle π). The Schmid factors, the angles π and $|\tau_{max}^{p}|$ for the $\{1\,1\,1\}\langle 1\,1\,0\rangle$ slip systems of grain G20/K computed from finite elements simulations are given in Table 3. Assessment of Table 3 and Fig. 12 proves that the two active slip systems are A6 (primary slip system) and D6 (secondary slip system). It is worth noting that D6 is the cross slip system of A6. Systematic studies on the nature of slip systems were successfully performed on 7 of 11 slip markings of type III. In the four other cases, only one slip marking direction was observed at magnification×25,000. These studies confirmed that the two slip marking directions observed in slip markings of type III correspond to the plane traces of both primary and cross slip systems. Interestingly, the resolved shear stress of the cross slip system was found between 0.33 and 1 times the resolved shear stress of the primary slip system. For the 11 cases, it was checked that the primary slip markings correspond to the primary slip system exhibiting the maximum resolved shear stress.

5. Discussion

5.1. Change in slip activity in the vicinity of a grain/twin boundary

The change in slip activity near the grain boundary was experimentally proved in the case of copper bicrystals [15,16]. Cubic elasticity induces stress heterogeneities near the grain boundaries. In this work, the profile of σ_{22}/Σ was found to vary when approaching the grain boundary for bicrystals. The variation depends on the orientation of the neighboring grain, namely misorientation, as previously exhibited by Sumigawa and Kitamura [17] for bicrystals and Sauzay [18] for polycrystals. It was also shown that it depends on the grain boundary angle compared to the uniaxial loading direction. These fluctuations results in change in the maximum resolved shear stress and consequently in slip activity near the grain boundaries. The profile of σ_{22}/Σ and $|\tau_{max}^{p}|$ were observed quite similar but some differences exist. The stress tensor triaxiality values were found different from 0.33 (the value for uniaxial stress state obtained remote the grain boundary) near the grain boundary. They were checked to be responsible for the differences between the profile of σ_{22}/Σ and $|\tau_{max}^{p}|$ in the vicinity of the grain boundary.

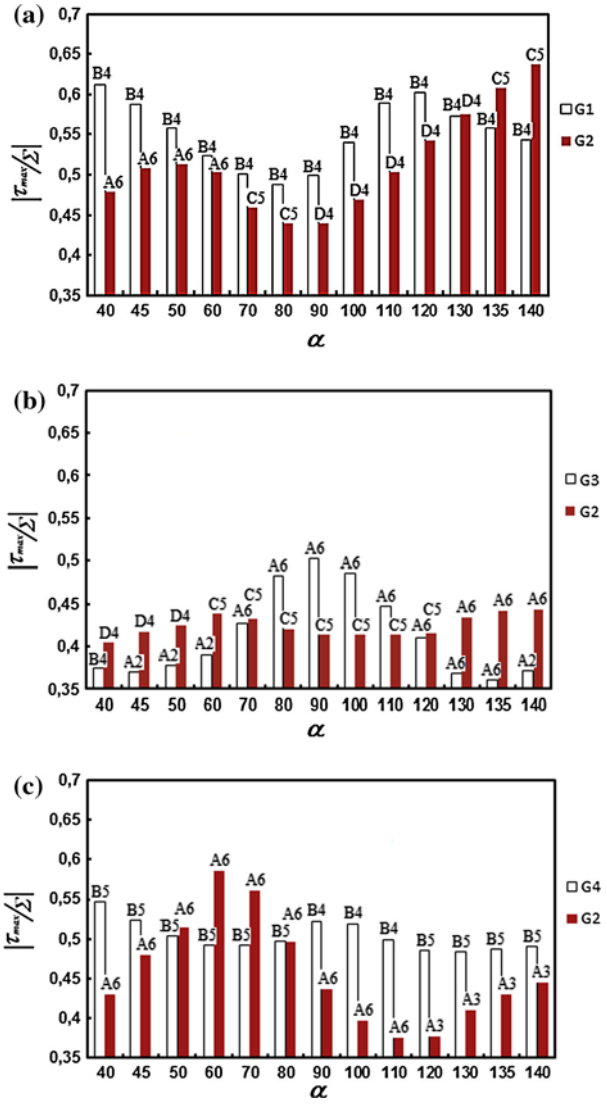

Fig. 8. Maximum resolved shear stress $|\tau_{max}{}^{P}|$ and active slip system at grain boundary in the middle axis of the front face for each grain belonging to bicrystal (a) G1–G2; (b) G3–G2 and (c) G4–G2.

Among all the studied grain boundary cases, the twin boundary for pure copper inclined ~45° (or equivalently ~135°) from the loading axis was found to lead to the highest resolved shear stress. It is thus preferential site for early slip activity. Two reasons explain such a result: (1) higher components of the local stress tensor due to strain incompatibilities related to cubic elasticity and (2) well-oriented slip system with the slip plane parallel to the twin boundary plane. These results are consistent with Sumigawa and Kitamura's previous works [17,19]. Combining experiments in high cycle fatigue with finite element simulation on copper bicrystals and multicrystals, they reported that twin boundaries were preferential sites for PSBs formation. PSBs were observed near and parallel to the twin boundary. The active slip system near the twin boundary was found different from that predicted by the Schmid factor.

Note that the configurations G1–G2 and $G1_{Twin}$–G2 for bicrystals are similar from a 2D point of view (same slip and grain boundary plane traces on the specimen surface). Section 4.1.3 revealed that accounting for the true 3D orientation of the twin boundary results in much higher resolved shear stress value. However, despite the fact that $|\tau_{max}{}^{P}|$ for $\alpha = 135°$ and grain G1–G2 is not the highest on the contrary to $G1_{Twin}$–G2 case, it belongs to the 0.55 > values in the [0.35–0.73] full range. Besides, the quasi 3D analysis successfully predicts location and the nature of the active slip systems near the twin/grain boundaries. As a result and for the sake of simplicity, only quasi 3D analysis (in the sense that the third direction was extruded from the specimen surface) was carried out to investigate slip markings criterion for real polycrystalline microstructure.

5.2. Slip markings criteria for copper polycrystals

For ductile single-phase metals, crack initiates along PSBs crossing the grains (slip markings of type I) in low and high cycle fatigues. PSBs appear in grains well-oriented for plastic slip and are aligned along the direction of the intersection line between the observed specimen surface and the primary slip system plane. The criterion based on the maximum Schmid factor (considering isotropic elasticity) successfully predicts the plastically deformed grain and the primary active slip system [7,8]. We found here that Schmid factor assessment cannot be used to predict nor locations of slip markings of types II and III neither the corresponding slip systems. The reason is that slip markings of types II and III are localized near grain/twin boundaries. As Schmid factor analysis considers the stress state as uniform, it cannot obviously predict the preferential occurrence of slip near grain/twin boundaries.

Maximum resolved shear stress (considering cubic elasticity) as a criterion for type II slip markings preferential sites was found 70% reliable criterion. It predicts the facts that twin boundaries inclined about 45° from the loading axis are the most preferential sites for slip markings nucleation at the early stage of plasticity. It also predicts that the active slip plane is parallel to the twin boundary plane. Slip markings along twin boundaries for polycrystals were also mentioned in literature for symmetrical strain-controlled fatigue tests operated at frequencies below 100 Hz, (i.e. much lower than the present frequency of 20 kHz) [17,19,20–22] confirming that the well-oriented twin boundaries promote very early slip and PSB formation.

Considering cubic elasticity, maximum resolved shear stress as a criterion for type III slip markings preferential sites was only found 30% reliable criterion. However, when there are slip markings, maximum resolved shear stress successfully predicts the primary active slip system. Slip markings of type III preferentially appear near twin boundaries and the primary slip plane is parallel to the twin boundary plane as for slip markings of type II. Slip markings of type III may also appear near large-angle grain boundaries and triple junctions, so in the highest stressed regions. These results show that high resolved shear stress is required to generate slip markings of type III but is not the sole reason explaining the presence of slip markings. Dislocation pile-ups and high geometrically necessary dislocation density at grain boundaries (and not taken into account in the present approach) may promote the emergence of slip markings of type III [23–25].

Using dynamic dislocation simulations, Robertson et al. [26] suggest another criterion to explain the presence of slip markings associated with slip systems having "low" resolved shear stress. The criterion is based on the so-called "surface connected volume". The "surface connected volume" corresponds to the portion of a grain from which dislocations can come out of the crystal, across the free surface, resulting, in principle, to emerging slip bands. The size of the surface connected volume associated with a given slip system is related to the angle β between the slip direction and the normal to the free surface (Fig. 1). Small angle β results in large surface connected volume. This concept is equivalent to the analysis based on type B PSB initiated by Brown and Miller [27] and gone back over by Sauzay and Gilormini [28]. The angle

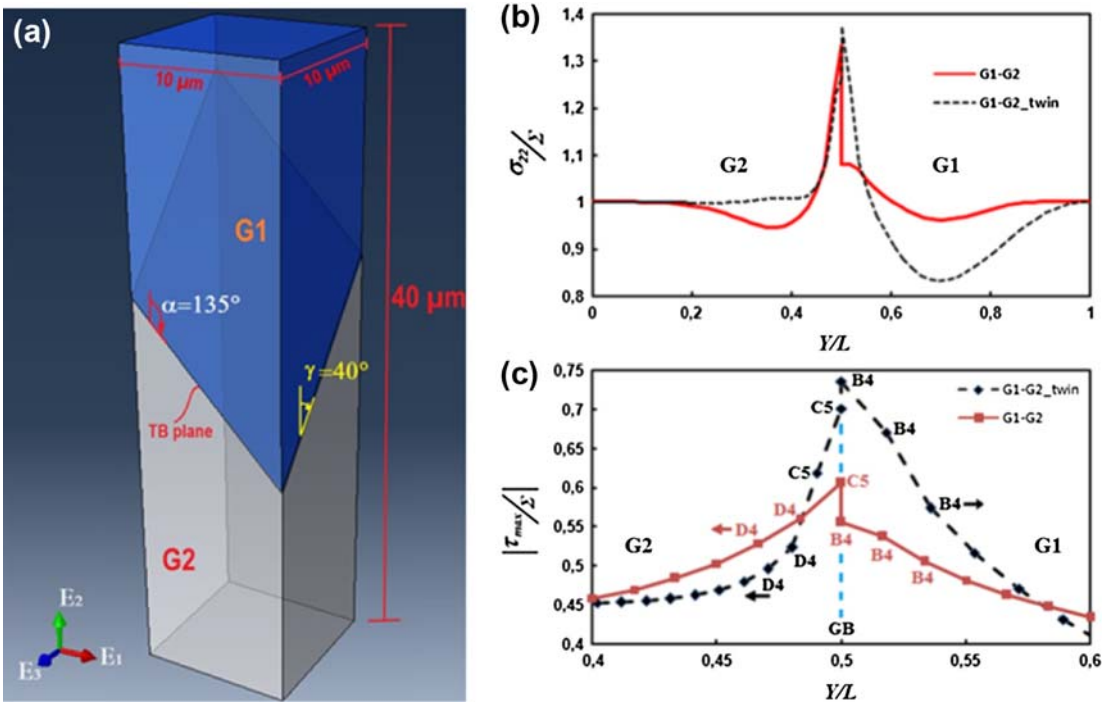

Fig. 9. (a) Geometry of the bicrystal $G1_{twin}$–G2; (b) profiles of σ_{22}/Σ and (c) $|\tau_{max}{}^{P}/\Sigma|$ near grain boundary along the middle axis of the front surface for bicrystals G1–G2 and $G1_{twin}$–G2.

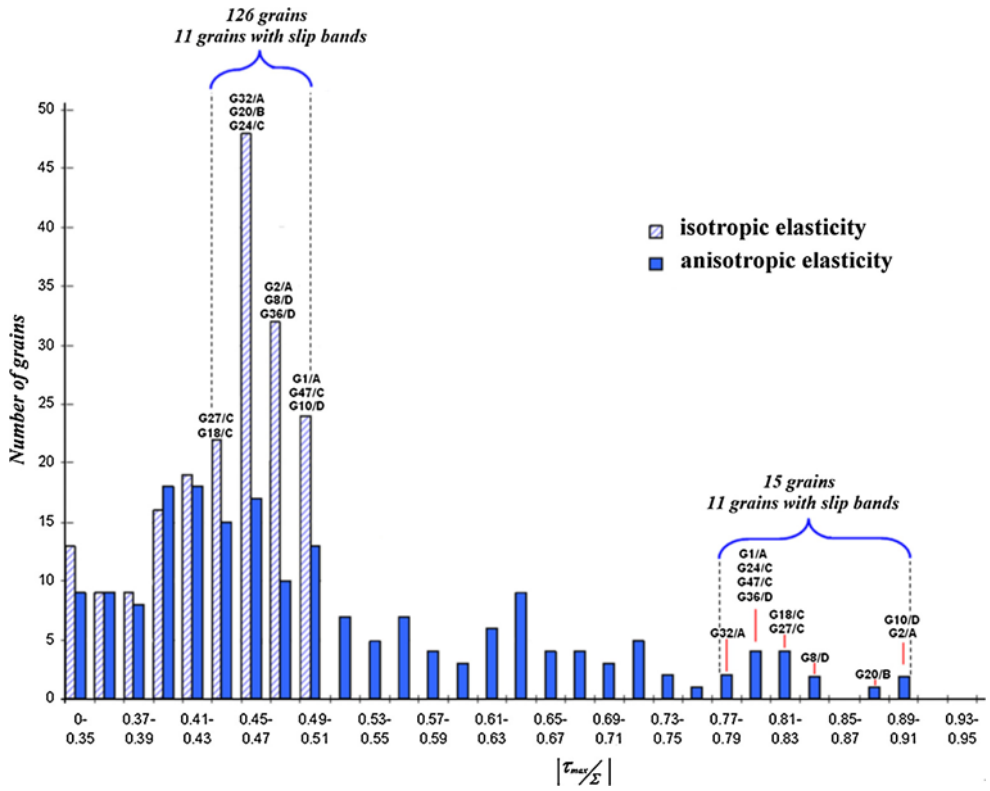

Fig. 10. $|\tau_{max}{}^{P}|$ Histogram over 192 grains contained into the four zones A, B, C and D – $|\tau_{max}{}^{P}|$ was calculated considering isotropic or anisotropic (cubic) elasticity to compute local stress tensor.

β associated with the slip markings of type II was found larger than 75° for 9 over 11 cases. For the slip markings of type III, it is greater than 45° for 10 over 11 cases. Our results are in good agreement with experimental results obtained on austenitic stainless steel in low cycle fatigue for slip markings crossing grains (labelled here as slip markings of type I) [29]. However, the large β values result in small surface connected volume and so, in principle, in no emerging slip bands (or at least emerging very weakly). Consequently, the large surface connected volume criterion clearly does not apply to the slip markings of types II and III.

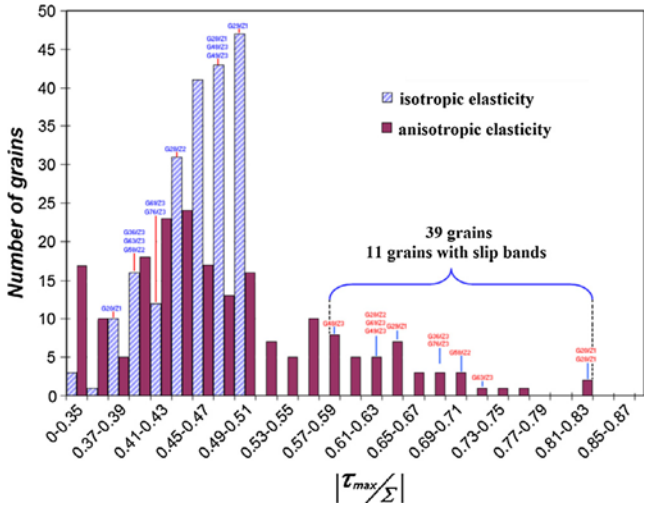

Fig. 11. $|\tau_{max}^{P}|$ Histogram over 204 grains contained into the three zones K, L and M. $|\tau_{max}^{P}|$ was calculated considering isotropic or anisotropic (cubic) elasticity to compute local stress tensor.

5.3. Relationship between the stress amplitude ranges and the appearance of slip markings

5.3.1. Estimation of the maximum resolved shear stress ranges associated with the type of slip markings

Considering that the four zones exhibiting slip markings of type II obtained after 10^7 cycles – $\Delta\sigma/2 = 56.4$ MPa and the three zones exhibiting slip markings of type III obtained after 10^8 – $\Delta\sigma/2 = 49.6$ MPa are representative of mechanical state for stress amplitudes below 65 MPa, the range of maximum resolved shear stress (averaged values over 1 μm × 1 μm) associated with slip markings was calculated: [43.7–50.7 MPa] for slip markings of type II and [29.3–41.2 MPa] for slip markings of type III. It is worth noticing that the calculated maximum resolved shear stresses may be different from the true values for three main reasons. Firstly, the localized plastic behavior in the slip markings emergence zone is neglected. The plastic behavior changes the stress heterogeneity. Steckmeyer et al. [30] showed that for nickel, the anisotropy coefficient of which is lower than but close to the copper one ($a = 2.5$ instead of $a = 3.3$), mainly cubic elasticity affects the stress heterogeneity up to 10^{-3} plastic strain. Besides, the active slip systems after a large number of cycles are generally already active at the beginning of the test [15]. The formation of the early slip markings (corresponding to plastic strain below 10^{-5} [4]) can thus be considered to be controlled by the stress heterogeneity due to the cubic elastic behavior. Secondly, the polycrystalline model is based on a quasi 3D microstructure involving columnar grains. Zeghadi et al. [31] studied the stress field for polycrystalline aggregates with different grain shapes and crystal orientations, except at one free surface where the 2D grain shape and initial lattice orientation were fixed. They found that the stress heterogeneity obtained for columnar grains is smoother than for random 3D synthetic microstructures but is rather similar to the ensemble average field in the case of cubic elastic behavior. Increasing the accuracy of the stress field estimation would require to explicitly represent the true 3D microstructure. Therefore, quasi 3D finite element simulation is a good compromise between the accuracy of the stress field at the free surface and the consuming time needed for 3D microstructure rebuilding [32]. Thirdly, the results were obtained with stress-controlled boundary conditions on two opposite surfaces. The four lateral surfaces were stress free surfaces. The true polycrystalline aggregates are located at the free surface and are embedded in the remaining grains. In order to estimate the impact of the boundary conditions on the results, the three lateral surfaces (except the observed specimen surface) were constrained to move in its perpendicular direction so that these surfaces were maintained flat. In both cases, the numerical simulations showed concentrations of the maximum resolved shear stress along some grain boundaries where the slip markings are observed in experiments. However, the stress concentrations were found much pronounced for the case of free surfaces than for the

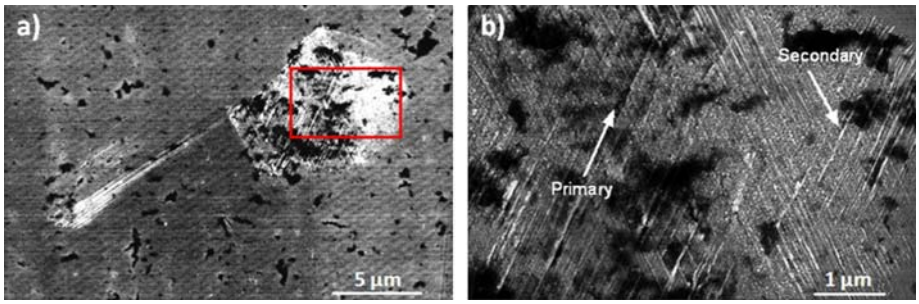

Fig. 12. SEM micrographs of slip markings of type III contained in the zone K observed from a specimen cyclically loaded up to 10^8 cycles at $\Delta\sigma/2 = 49.6$ MPa using a 20 kHz – ultrasonic fatigue device. The loading axis is vertical.

Table 3
Schmid factors, angles π and $|\tau_{max}^{P}|$ for the grain G20/K exhibiting slip markings of type III with two marking directions. The primary and cross-slip systems are printed in bold.

G20/K primary slip marking-measured $\pi = 28°$/secondary slip markings-measured $\pi = 156°$												
	B5	B4	B2	**A6**	A3	A2	**D6**	D4	D1	C5	C3	C1
R_{22}	−0.01	−0.16	−0.15	**−0.32**	0.05	0.37	**−0.25**	0.31	0.06	0.06	0.11	0.17
π	123°	123°	123°	**28.6°**	28.6°	28.6°	**156°**	156°	156°	94.5°	94.5°	94.5°
$\lvert\tau_{max}^{P}\rvert$	0.02	0.29	0.31	0.6	0.00	0.58	0.55	0.53	0.02	0.05	0.24	0.29

case of constrained surfaces. The maximum difference of the maximum resolved shear stress was found of about 30% at these specific locations.

Despite the hypotheses discussed above, the minimum value of $|\tau_{max}|$ in the range [29.3–41.2 MPa] for slip markings of type III was found close to the PSB threshold (28 MPa) defined as the shear stress at the plateau of the cyclic stress–strain curve for copper single crystal oriented for single slip [33,34]. It is also above the critical shear stress associated with cross slip for pure copper at room temperature (24.5 MPa at 293 K [35]). Most of slip markings of type III exhibit traces of the primary and cross slip systems. No slip markings were observed below 29.3 MPa. These results suggest that the cross slip plays a key role in the slip markings emergence.

5.3.2. Scenario for slip markings formation

Based on the present and literature results, a scenario for type III slip markings formation is suggested in this section. At the beginning of the fatigue tests for stress amplitudes below 45 MPa for which most of early slip markings are of type III, the local stress state enables the homogenous but slight activation of dislocation sources or the mobility of the existing dislocation in grains since the local resistance is very low (few MPa [36,37]). Cross slip events are significantly activated at higher stresses (above about 30 MPa). Consequently, primary slip system is very likely activated in the whole grain while cross-slip events take place only at the highest stress regions such as twin boundaries, highly misoriented grain boundaries or triple junctions because of elastic strain incompatibilities and dislocation pile-ups. Cross slip essentially contributes to dislocation storage and microstructure as shown experimentally [37] or by discrete dislocation dynamics modeling [38,39]. It results to strain localization and makes slip not completely recoverable leading to slip markings on the specimen surface. Using discrete dislocation dynamics modeling for 316 steel, Déprés et al. [40] concluded that, despite cross slip is essential for dislocation microstructure formation in fatigue, it does not contribute to plastic deformation. So, the primary slip system accumulates most plastic deformation. In the present case, the slip markings of type III were observed in the highest stressed regions where the cross slip can be activated. The presence of slip markings associated with the cross slip plane proves that the cross slip system contributes to plastic deformation but very less than the primary slip system for which slip markings are much more marked [6]. These findings suggest that the critical shear stress associated with cross slip governs the critical shear stress for slip markings appearance.

For higher stress amplitudes (typically in the 45–65 MPa range), predominantly slip markings are no more of type III but are of type II. When stress amplitude increases but remains lower than 65 MPa, the cross-slip probability increases but mainly near well-oriented twin boundaries as the maximum resolved shear stress steeply decreases when moving away from the twin boundary. Therefore, in these regions, strain localization starts earlier and likely right from the beginning of the cycles. Intense slip bands form. They enable strong strain accommodation while reducing stored energy [33,40]. As a result, ~1 μm height isolated slip bands emerge in the vicinity of well-oriented twin boundaries on the specimen surface. This scenario explains the presence of early slip markings of type II and the absence of slip markings of type III in the [45–65 MPa] stress amplitude range. For stress amplitudes >65 MPa, local stresses are high enough to generate cross slip events in the whole well-oriented grain producing slip markings of type I, commonly observed in low and high cycle fatigue. This scenario clarifies the stress amplitude conditions to observe slip markings of types I, II or III as early slip markings in VHCF for copper polycrystals. Besides, it is consistent with Phung's et al. [6] observations which suggest that the slip markings of type III change into the type I or type II over cycles. With increasing the number of cycles, the slip markings of type III for which the primary slip plane corresponds to the twin boundary plane were found to confine and grow into more intense slip markings, similar to the slip markings of type II [6]. The clusters of slip markings of type III for which the primary slip plane does not correspond to a twin boundary plane were found to exhibit more pronounced slip markings space out 5–10 μm as the type I slip markings [6]. Déprés et al. [41] investigated the surface slip markings evolution over cycles using dynamic dislocations simulations. Their analysis and our scenario can explain both phenomena: the cross slip activity gradually progresses over cycles leading to more and more strain localization and intense and slip markings separated from each other.

6. Conclusion

Using finite element simulations and considering crystalline cubic elasticity, it was shown that:

- Schmid factor criterion is not valid for predicted preferential sites of slip markings of type II and III and the corresponding primary active slip systems.
- Considering cubic elasticity, maximum resolved shear stress as a criterion for type II slip markings preferential sites is 70% reliable criterion. Concerning slip markings of type III, the reliability falls to 30%.
- Well-oriented twin boundaries are indeed preferential sites for appearance of early slip markings of types II and III in fatigue at very low stress amplitudes because of strong stress concentrations due to cubic elasticity and the existence of well-oriented slip planes parallel to the twin boundary plane.
- Slip markings of type III also appear near large-angle grain boundaries and triple junctions. When two slip markings direction exist, they are associated with the planes of the primary and cross slip systems.
- The critical shear stress associated with cross slip was suggested to govern the critical shear stress for slip markings appearance.
- A scenario rationalizing the stress amplitude conditions and sites to observe slip markings of types I, II or III as early slip markings in VHCF for copper polycrystals was proposed.

Acknowledgements

We would like to acknowledge the Agence Nationale de la Recherche France ANR-09-BLAN-0025-01 for the funding that enabled this work to be carried out. They would like to also acknowledge Professor Haël Mughrabi and Doctor Maxime Sauzay for their very helpful comments. This paper is dedicated to Doctor Thierry Bretheau, Director of Research at CNRS who suggested the role of crystalline anisotropic elasticity in microplasticity occurring in very high cycle fatigue.

References

[1] Ranc N, Wagner D, Paris PC. Study of thermal effects associated with crack propagation during very high cycle fatigue tests. Acta Mater 2008;56:4012–21.
[2] Mughrabi H. On multi-stage fatigue life diagram and the relevant life controlling mechanisms in ultra-high cycle fatigue. Fatigue Fract Eng Mater Struct 2002;25:755–64.
[3] Mughrabi H. On the life-controlling microstructural fatigue mechanisms in ductile metals and alloys in the gigacycle regime. Fatigue Fract Eng Mater Struct 1999;22:633–41.
[4] Stanzl-Tschegg S, Mughrabi H, Schönbauer B. Life-time and cyclic slip of copper in the VHCF-regime. Int J Fatigue 2007;29:2050–9.

[5] Stanzl-Tschegg SE, Schönbauer B. Mechanisms of strain localization, crack initiation and fracture of polycrystalline copper in the VHCF regime. Int J Fatigue 2010;32:886–93.
[6] Phung NL, Favier V, Ranc N, Vales F, Mughrabi H. Very high cycle fatigue of copper: evolution, morphology and locations of surface slip markings. Int J Fatigue 2014;63:68–77.
[7] Blochwitz C, Brechbühl J, Tirschler W. Analysis of activated slip systems in fatigued nickel polycrystals using the EBSD-technique in the scanning electron microscope. Mater Sci Eng A 1996;210:42.
[8] Aubin V, Sabatier L, Villechaise P, El Bartali A. Identification and analysis of slip systems activated during low-cycle fatigue in a duplex stainless steel. Scr Mater 2008;59:1231–4.
[9] Phung NL, Marti N, Blanche A, Ranc N, Favier V, Chrysochoos A, et al. Very high cycle fatigue for single phase ductile materials: slip band appearance criterion. Proc Eng 2013;66:615–25.
[10] Schmid E, Boas W. Plasticity of crystals. London: Hughes; 1950.
[11] Iida S, Ohno K, Kamimae H, Kumagai H. Tables of physical constants, 1992. p. 24.
[12] Kocks UF, Tomé CN, Wenk HR. Texture and anisotropy, 2000.
[13] Leguillon D, Sanchez-Palancia E. On 3D cracks intersecting a free surface in laminated composites. Int J Fract 1999;99:25–40.
[14] Bunge HJ, Esling C. Quantitative texture analysis. Oberursel: DGM-Informationsgesellschaft; 1981.
[15] Méric L, Cailletaud G, Gaspérini M. FE calculations of copper bicrystal specimens submitted to tension-compression tests. Acta Metall Mater 1994;42:921–35.
[16] Hu YM, Wang ZG. Grain boundary effect on the fatigue deformation and cracking behaviour of copper bicrystals. Int J Fatigue 1998;20:463–9.
[17] Sumigawa T, Kitamura T. Nucleation of slip bands near twin boundary in high-cycle fatigue. Trans Jpn Soc Mech Eng 2004;68:1104–11.
[18] Sauzay M. Cubic elasticity and stress distribution at the free surface of polycrystals. Acta Mater 2007;55:1193–202.
[19] Kitamura T, Sumigawa T, Ohishi K. Slip behavior and local stress near grain boundary in high-cycle fatigue of copper polycrystal. Trans Jpn Soc Mech Eng 2001;67:1819–24.
[20] Neumann P, Tönnessen A. Crack initiation at grain boundaries in FCC materials – strength of metals and alloys, vol. 1. Oxford: Pergamon Press; 1988. p. 748.
[21] Peralta P, Laird C, Mitchell TE. Fatigue fracture at copper bicrystal interfaces: fractography. Mater Sci Eng A 1999;264:215–31.
[22] Polak J, Vasek A. Fatigue damage in polycrystalline copper below the fatigue limit. Butterworth-Heinemann publisher; 1994.
[23] Ashby MF. The deformation of plastically non-homogeneous materials. Philios Mag 1970;21:399–424.
[24] Li JCM, Chou YT. The role of dislocations in the flow stress grain size relationships. Metall Trans 1970;1:1145–59.
[25] Jiang J, Britton TB, Wilkinson AJ. Evolution of dislocation density distributions in copper during tensile deformation. Acta Mater 2013;61:7227–39.
[26] Robertson CF, Déprés C, Fivel M. The effect of mean stress and thermo-mechanical induced stress on micro-crack initiation: an analysis based on experiments and DD simulation results. Mater Sci Forum 2008;567–568:89–92.
[27] Brown MW, Miller KJ. A theory for fatigue failure under multiaxial stress–strain conditions. Proc Inst Mech Eng 1973;187:65–73.
[28] Sauzay M, Gilormini P. Influence of surface effects on fatigue of microcracks nucleation. Theor Appl Fract Mech 2002;38:53–62.
[29] Mu P, Aubin V, Alvarez-Armas I, Armas A. Influence of the crystalline orientations on microcrack initiation in low-cyclefatigue. Mater Sci Eng A 2013;573:45–53.
[30] Steckmeyer A, Sauzay M, Weidner A, Hieckmann E. Micromechanical modelling of the cyclic stress–strain behaviour of nickel. Int J Fatigue 2012;40:154–67.
[31] Zeghadi A, N'Guyen F, Forest S, Gourgues AF, Bouaziz O. Ensemble averaging stress–strain fields in polycrystalline aggregates with a constrained surface microstructure – Part 1 anisotropic elastic behaviour. Philos Mag 2007;87:1401–24.
[32] Qidwai SMA, Lewis AC, Geltmacher AB. Using image-based computational modeling to study microstructure–yield correlations in metals. Acta Mater 2007;55:4121–36.
[33] Mughrabi H. The cyclic hardening and saturation behaviour of copper single crystals. Mater Sci Eng A 1978;33:207–23.
[34] Laird C, Charsley P, Mughrabi H. Mater Sci Eng 1986;81:433–50.
[35] Bonneville J, Escaig B, Martin J. A study of cross-slip activation parameters in pure copper. Acta Metall 1988;36:1989–2002.
[36] Vellaikal G. Some observations on microyielding in copper polycrystals. Acta Metall 1969;17:1145–54.
[37] Basinski SJ, Basinski ZS, Howie A. Early stages of fatigue in copper single crystals. Philos Mag 1969;19. 899–824.
[38] Devincre B, Kubin LP. Mesoscopic simulations of dislocation and plasticity. Mater Sci Eng A 1997;234–236:8–14.
[39] Déprés C, Robertson C, Fivel M. Crack initiation in fatigue: experiments and three-dimensional dislocation simulations. Mater Sci Eng A 2004;387–389:288–91.
[40] Déprés C, Fivel M, Robertson C. Low-strain fatigue in AISI 316L steel surface grains: a three-dimensional discrete dislocation dynamics modelling of the early cycles I. Dislocation microstructures and mechanical behaviour. Philos Mag 2004;84:2257–75.
[41] Déprés C, Robertson C, Fivel M. Low-strain fatigue in 316L steel surface grains: a three dimension discrete dislocation dynamics modelling of the early cycles. Part 2: persistent slip markings and micro-crack nucleation. Philos Mag 2006;86:79–97.